Novel Hydrothermally Synthesized Strontium Telluride Nanoballs as: Efficient Electrocatalyst for Oxygen Evolution Reaction

F. F. Alharbi
Sumaira Manzoor
Mehar Un Nisa
Abdul Ghafoor Abid
Salma Aman
Muhammad Naeem Ashiq (naeembzu@bzu.edu.pk)

Research Article

Keywords: Strontium telluride, Oxygen evolution reaction, Nanoballs, Water splitting.

Posted Date: February 23rd, 2022

DOI: https://doi.org/10.21203/rs.3.rs-1370161/v1

Version of Record: A version of this preprint was published at JOM on June 10th, 2022. See the published version at https://doi.org/10.1007/s11837-022-05362-5.

Abstract

The engineering of extremely efficient, low-cost, and stable electrocatalysts were required for the sluggish oxygen evolution reaction (OER). Herein, using hydrothermal technique, strontium telluride (SrTe/GC) nanoballs fabricated for water splitting to work efficiently as an efficient OER catalysts. According to physical and chemical characterizations, SrTe/GC nanoballs exhibits a three-dimensional form and homogeneous surface distribution, performing a low overpotential of 268 mV at 10 mA/cm^2 with small Tafel slope of 25 mV/dec. The fabricated material exhibits excellent stability of 24 hours with no decline in current density. The Te-induced metallic telluride and substantial covalency around the strontium center is responsible for this catalyst's outstanding performance. This study reveals the valuable insight of metal telluride materials to function as an extraordinarily efficient and stable OER catalysts at high current densities.

1. Introduction

Fossil fuels now account for the vast majority of the world's energy [1], and these energy carriers must be phased out due to their rapid depletion, environmental contamination, and carbon footprints. To compete with fossil fuels, scientists are exploring new renewable energy sources [2]. Long-term energy allocation is getting increasingly difficult as energy distribution networks grow more efficient [3], and if energy is available indefinitely, an increase in industrial output is achievable [4]. The electron transfer process allows the renewable energy to be stored in chemical bonds [5–7]. Renewable energy sources include biofuels, solar electricity, wind power, and water power [8, 9]. Because of its great efficiency and low environmental impact, hydrogen (H_2) is often promoted as a potential option to meet the growing global demand for clean and renewable energy resources [10–13]. On the one hand, finding a cost-effective, convenient, and ecologically friendly means to obtain H_2 gas [14–16]. It was created in reaction to an imminent primary resource shortage, as well as the low conversion efficiency and environmental concerns [17, 18]. When using renewable energy sources like wind [19], geothermal [20], and solar power [21], electrochemical water splitting has proven to be a viable choice among many others [22–24]. One of a number of alternatives, oxygen evolution (OER) and hydrogen evolution (HER) processes can be used in a variety of ways to electrolyze the water [25–27].

The practical results for electrolytic polarization-induced overpotentials (e.g. 1.50 V) are sometimes substantially different from theoretical expectations (1.23 V) [28, 29]. When it comes to improving reaction rates on a large scale, commercial application of precious metal electrocatalysts like IrO_2/RuO_2 for OER and Pt-based materials for HER is limited by high costs, lack of availability, and monotonous activity [30–32]. There has been ongoing research into metal-based materials such as oxides and hydroxides, phosphides, nitrides, and carbides [33–35]. There are various advantages to using OER electrocatalysts, which can sustain activity and stability in alkaline electrolytes while lowering capital and operating expenses [36]. At alkaline concentrations, however, OER electrocatalysts struggle to maintain their high activity and long life [37]. If electrocatalysts are to be effective, they must consider a number of

criteria, like charge transfer to surface reaction sites is enabled by electrocatalysts with higher electric conductivity than the substrate electrodes [38]. In order to provide more readily accessible active zones for higher currents, they must have a larger specific surface area than substrate electrodes [39]. To lower activation energy, electrocatalysts must change their hierarchical structure. This can be accomplished by altering the electrocatalysts' chemical and physical properties. The chemistry and electrical conductivity of an electrocatalytic surface active site can be fine-tuned to some extent. The easiest technique to enhance the number of active sites and mass diffusion capacity of electrocatalysts is to make them porous [40]. One of the most promising catalysts is porous materials, which have demonstrated their efficiency in a range of chemical reactions [41]. Because of their distinct physical and chemical properties, porous materials have a number of benefits over bulk materials when it comes to water-splitting electrocatalysts [42, 43].

In an effort to increase the electrochemical performance, metal chalcogenides-based electrode materials have recently been investigated [44], and outperform their micron-sized equivalents in terms of performance. Higher quantities of surface oxygen binding energy are required for OER activity. The telluride based material has received little attention for OER catalysis, despite its metallic nature [45]. As a result, metal tellurides have better electrical conductivity, mechanical strength, rate capability, and cycling stability due to their synergistic benefits [46]. As far as we know, no one has ever employed hydrothermal synthesis to produce SrTe as an electrocatalyst to improve the electrochemical activity or electrode material durability. Due to the presence of telluride, the strontium tellurides exhibit high specific capacitance and a high level of stability. The electrochemical characteristics of synthesized catalyst is exceptional because of their more active sites, ion dispersion, and enhanced electron transmission may be expedited, and all the activities are discussed below.

2. Experimental Section

2.1. Materials

Analytical-grade chemicals as such were used to make strontium telluride. Deionized water (resistivity = 18.2 M cm) was used to make all of the solutions in this experiment, and the following chemicals were utilized in the experiment like Tellurium powder (Te, > 99.9%), Strontium nitrate ($Sr(NO_3)_2.6H_2O$, Sigma Aldrich, > 99.9%), Hydrazine monohydrate, ($N_2H_4.H_2O$, Panreac, > 80%), Ethyl alcohol (Merck, 99.8%), and Potassium hydroxide (KOH, Analar, 99%).

2.2. Preparation of SrTe

Ordinary conditions and significantly simple setup were employed for hydrothermal synthesis to generate SrTe nanoballs. Dissolving 5 mL of 7 M KOH solution in 0.01 M strontium nitrate hexahydrate and 0.01 M tellurium powder for the synthesis of SrTe. The mixture must be homogenized for two hours with the addition of 2 mL of hydrazine monohydrate. The resultant mixture was placed in 100 ml Teflon-sealed stainless-steel autoclave at 180°C for 12 hours. To separate precipitates and impurity elimination, it was

centrifuged after being filtered through deionized water and ethanol subsequently. Finally, the material was dried in a preheated oven at 70°C overnight, and the obtained SrTe powder was stored for characterization purpose.

2.3. Characterization

A Bruker D_2 PHASER powder diffractometer with Ni-filtered CuK radiation at 30 kV and a current of 10 mA was utilized for the XRD study. On a $2\boldsymbol{\theta}$ scale of 20–80^o, scans were done at a rate of 5^o min^{-1}. Scanning electron images taken with the Quanta 200-FEG SEM reveal the morphologies of the samples. Transmission electron microscope (JEOL (JEM-2100) TEM) was used also to analyze the deep internal morphology.

2.4. Electrochemical setup

In a Teflon-covered Pyrex glass cell with 1.0 M KOH solution was employed via three-electrode electrochemical cell to perform cyclic voltammetry, electrochemical impedance spectroscopy, and controlled potential bulk electrolysis. The electrochemical cell was cleaned thoroughly with ultrapure water and acetone before being utilized and then dried at 80°C for around 30 minutes. HNO_3: HCl (1:3) as a cleaning solution was utilized for Ag/AgCl and platinum wire, employed as reference, and counter electrodes in the as-prepared electrode system. Before being used in the electrochemical cell, the platinum wire was cleaned in a nitric acid solution. As specified in the equation, all potential measurements were taken using a reversible hydrogen electrode (RHE).

$E_{RHE} = E_{Ag/AgCl} + E_o + (0.059*pH)$ (1)

To compensate for their 50% iR-compensation, the cyclic and linear sweep voltammeteries were scanned at 5 mV/s. The electrochemical cell containing the electrolyte was cleansed with argon gas for around 30 minutes, and the geometrical area of the working electrode was used to compute all current densities. Using the following equation like to determine the Tafel slope to learn more about catalytic and kinetic efficacy.

$\eta = \alpha + 2.303 \frac{RT}{\alpha nF} \log j$ (2)

The number of electrons involved in this reaction is n, the Faraday constant is F, current density is j, and the slope is 2.303 RT/nF. Using the Cyclic Voltammetry (CV) curve in the non-faradic zone at different scan speeds, the capacitance of the as-prepared working electrodes' double layer was determined at a scan rate of 2, 4, 6, and 8 mV/s. To calculate the ECSA of the synthesized electrode material, divide the capacitance of the double layer by a constant of 0.04 mFcm^{-2}.

$ECSA = C_{dl}/C_s$ (3)

Electrochemical impedance (EIS) spectroscopy was used to measure the interphase solution and charge transfer resistances across an electrode-electrolyte interface (0.1 Hz to 100,000 Hz frequency range). In

the high frequency range, this method is related to the Nyquist plot Z' against -Z”s semicircle diameter. NOVA 2.1 software and a simple Randles circuit were used to calculate the Rs and Rct from Metrohm Autolab electrochemical workstation. Each cyclic voltammetry curve has been IR adjusted to the possible greatest extent. To account for potential values, use the following equation:

$E_{actual} = E_{experimental} - IR$ (4)

3. Results And Discussion

3.1. Structural analysis

A simple hydrothermal procedure for manufacturing SrTe/GC nanoballs are shown in Fig, 1. The crystal structure and purity of SrTe/GC was found by XRD investigation. Figure 1 depicts the results of sample used to identify the crystalline phases and product composition are well matched with Joint committee of powder diffraction (JCPDS) card No. 03–065–5700 (space group: Pm-3m, space group number: 221). All peaks correspond to the Cubic crystalline SrTe/GC phases make up the end product. Strontium based telluride diffraction peaks at $2\boldsymbol{\theta}$ = 24.1º, 34.5 º, 42.3 º, 49.2 º, 55.4 º, 61.1 º, 72.1 º, and 77.3 º indexed to hkl (100), (110), (111), (200), (210), (211), (220), and (221) are well matched revealing high purity and narrow intense peak display crystallization.

3.2. Morphological analysis

Scanning electron microscopy (SEM) image reveals the morphology of SrTe/GC displaying small, cluster nanoballs (Fig. 2a&b). The morphology of nanoballs with varying size can be visualized using SEM images (Fig. 2a). As observed in the SEM photos, the nanoballs had average thickness of 40 nm. Ultra-small structure may exhibit large number of active sites to electrolytes for the ease of ions and electron transportation across the interface of the electrode and electrolyte. The transmission electron (TEM) image shown in (Fig. 2b) is well in agreement and consistent with the SEM micrograph. The TEM is in enlarged as compared to the SEM micrograph considering large active sites for better oxygen evolution reaction.

3.3. Electrochemical characterization

The OER was carried out at a scan rate of 5 mV/s in an electrolyte containing 1.0 M KOH catalyzed by SrTe/GC balls deposited on glassy carbon (GC) electrodes to obtain CV curves for catalyst effectiveness study as shown in Fig. 3a. SrTe/GC has a high integrated peak area, implying that many Sr-charged species are involved in the generation of oxygen gas. The anodic peak value of the Sr redox reaction for SrTe/GC at 1.48 V vs RHE and overpotential of 268 mV at 10mA/cm^2 current density through the CV and LSV are shown in Fig. 3a-b. The CV curve for SrTe/GC, exhibits an effective OER swing, enhanced current density, and decreased overpotential due to the formation of hydroxotelluride and oxyhydrotelluride in alkaline media. The sharp and steep peak confirms the active strontium ions as result intermediate of hydroxotelluride and peroxide produces to speed up the sluggish oxygen evolution reaction. Because

induction of strontium in chalcogenide may influence the lattice structure and engineering morphology, resulting in increased OER activity. Table 1 shows the comparative study of all electrochemical activity with SrTe/GC balls. The exceptional OER activity of unimetal with telluride make it superior rather than using bimetallic chalcogenides with same results.

Electrochemical impedance is one of the techniques to measure the intrinsic electrocatalytic activity. The EIS test shown in Fig. 3(c) for the SrTe/GC electrocatalyst exhibits low charge transfer resistance (R_{ct}) and solution resistance (R_s) that is 3.5 and 3.2 Ω, respectively. The semicircle in a low frequency region demonstrates small resistance to charge transfer and high electrical conduction for the smooth OER performance. Because of the low Rct value, electrons are quickly transferred from the electrolyte to the electrode.

For better understanding the kinetics of the electrochemical water oxidation, tafel slope is computed from the linear component of the CV shown in Fig. 3(d). The OER kinetics of SrTe/GC nanoballs appear to be superior due to its smaller tafel slope 25mV comparable to or lower than previously reported metal telluride-based electrodes (Table 1). Simple electron transfers and rate-determining steps have long been associated with the Tafel slope. According to the tafel slope, there is 4 electron transfer for the OER rate determining step. The SrTe/GC tafel slope value indicates that oxygen evolution occurs faster during electrochemical reaction.

$SrTe+OH^- \rightarrow SrTe\text{-}OH^- + e^-$ (5)

$SrTe\text{-}OH+OH^- \rightarrow SrTe\text{-}O+H^+ + e^-$ (6)

$SrTe\text{-}O+OH^- \rightarrow SrTeOOH+e^-$ (7)

$SrTe\text{-}OOH+OH^- \rightarrow SrTe+O_2+H^+ + e^-$ (8)

Table 1: Comparison of different electrocatalysts with the present study

Sr. No.	Electrocatalyst	Over potential (mV) at $10mAcm^{-2}$	Tafel slope ($mVdec^{-1}$)	References
1	CoTe	241	66	[47]
2	MOF/$CoTe_2$	330	61.67	[48]
3	$CoTe_2$-$MnTe_2$	310	115	[49]
4	$CuTe_2$	323	96	[50]
5	Porous NiTe	679	151	[51]
6	Cu_7Te_4	460	103	[52]
7	**SrTe**	**268**	**25**	**This work**

Total four CV cycles at different scans rates (2, 4, 6, and 8 mV/s) were performed in a short voltage in the non-faradic region as shown in Fig. 4a. Hierarchical poriferous nanoballs have a densely packed electrochemical surface area with active patches. Double layer capacitance is used to calculate the ECSA. The integrated area of the CV curve in the range of -0.6 to 0.8 V vs. RHE has slightly increased, as seen by the CV curves in Fig. 4a. With a C_{dl} value of 33.5 cm^{-2} at a potential window of -0.6 to 0.8 V against RHE, these hierarchical nanoballs had the most electrochemically active surface area (Fig. 4b). As a result, surface averaged techniques can be utilized to assess electrocatalysis' intrinsic activity. To evaluate intrinsic catalytic activity, LSV curves can be normalized with electrochemical active surface area (ECSA). The ultrasmall SrTe/GC nanoball increases mass transport kinetics by increasing the contact area between the electrode and the electrolyte, resulting in faster charge transfer. Conductivity is higher in SrTe due to fast transport kinetics across the electrode-electrolyte interface are achievable due to the high conductivity generated during the oxygen evolution event, as indicated by the low onset, overpotential, tafel slope and charge transfer resistance. The electrocatalyst's long-term stability is determined by its ability to be used in real-world applications.

Using repeated CV scans under the same electrochemical conditions, the long-term survival of an electrocatalyst was examined. In a 1.0 M KOH solution, the first and 1000th CV cycles at 50 mV/sec provide the almost same electrochemical signal as repeated CV scans (Fig. 5) In strongly oxidative circumstances, the CV cycle shows that catalytic function is slightly affected. Slight decrease in current density and no change in onset potential is observed. Hence, the nanostructures are suitable for large-scale commercial applications because they can penetrate and eliminate gas bubbles from the electrode edge.

4. Conclusion

Simple hydrothermal technique was used to synthesize the nanosized strontium telluride (SrTe) with a ball-like structure and are analyzed with different techniques. OER activity of the synthesized material is high due to the three-dimensional structure, enhanced electrochemical surface area resulting 1.48 V onset and 268 mV overpotentials to attain 10 mA/cm^2 current density. A moderately steep Tafel slope (25 mV/dec) for 4 electron coupled proton transfer. Also, the catalyst is extremely stable after 24 hours at a constant current density. This research looks at the viability of synthesizing metallic telluride with a certain shape, high activity, and stability at high current densities to increase OER performance and produce high purity H_2 on a large scale.

Declarations

Acknowledgement

The authors express their gratitude to Princess Nourah bint Abdulrahman University Researchers Supporting Project (Grant No. PNURSP2022R55) Princess Nourah bint Abdulrahman University, Riyadh Saudi Arabia

References

1. Tyedmers, P.H., R. Watson, and D. Pauly, *Fueling global fishing fleets.* AMBIO: a Journal of the Human Environment, 2005. **34**(8): p. 635-638.
2. Brockway, P.E., et al., *Estimation of global final-stage energy-return-on-investment for fossil fuels with comparison to renewable energy sources.* Nature Energy, 2019. **4**(7): p. 612-621.
3. Handayani, K., Y. Krozer, and T. Filatova, *From fossil fuels to renewables: An analysis of long-term scenarios considering technological learning.* Energy policy, 2019. **127**: p. 134-146.
4. Hickel, J. and G. Kallis, *Is green growth possible?* New political economy, 2020. **25**(4): p. 469-486.
5. Gao, C., et al., *Heterogeneous single-atom catalyst for visible-light-driven high-turnover CO2 reduction: the role of electron transfer.* Advanced Materials, 2018. **30**(13): p. 1704624.
6. Seselj, N., et al., *Tailored electron transfer pathways in Aucore/Ptshell–graphene nanocatalysts for fuel cells.* Advanced Energy Materials, 2018. **8**(13): p. 1702609.
7. Nong, H.N., et al., *Key role of chemistry versus bias in electrocatalytic oxygen evolution.* Nature, 2020. **587**(7834): p. 408-413.
8. Fraundorfer, M. and F. Rabitz, *The Brazilian renewable energy policy framework: Instrument design and coherence.* Climate Policy, 2020. **20**(5): p. 652-660.
9. Pratiwi, S. and N. Juerges, *Review of the impact of renewable energy development on the environment and nature conservation in Southeast Asia.* Energy, Ecology and Environment, 2020. **5**(4): p. 221-239.
10. Pivovar, B., N. Rustagi, and S. Satyapal, *Hydrogen at scale (H2@ Scale): key to a clean, economic, and sustainable energy system.* The Electrochemical Society Interface, 2018. **27**(1): p. 47.
11. Oliveira, A.M., R.R. Beswick, and Y. Yan, *A green hydrogen economy for a renewable energy society.* Current Opinion in Chemical Engineering, 2021. **33**: p. 100701.
12. Dincer, I. and C. Acar, *Smart energy solutions with hydrogen options.* International Journal of Hydrogen Energy, 2018. **43**(18): p. 8579-8599.
13. Gautam, P., S. Kumar, and S. Lokhandwala, *Energy-aware intelligence in megacities*, in *Current developments in biotechnology and bioengineering*. 2019, Elsevier. p. 211-238.
14. Hassan, I., et al., *Hydrogen storage technologies for stationary and mobile applications: Review, analysis and perspectives.* Renewable and Sustainable Energy Reviews, 2021. **149**: p. 111311.
15. Xiang, M., et al., *Accelerating Hydrogen Evolution by Anodic Electrosynthesis of Value-Added Chemicals in Water over Non-Precious Metal Electrocatalysts.* ChemPlusChem, 2021. **86**(9): p. 1307-1315.
16. Zhang, J., et al., *Recent progress for hydrogen production by photocatalytic natural or simulated seawater splitting.* Nano Research, 2020. **13**(9): p. 2313-2322.
17. Chen, J., et al., *Assessment of supercritical water gasification process for combustible gas production from thermodynamic, environmental and techno-economic perspectives: a review.* Energy

Conversion and Management, 2020. **226**: p. 113497.

18. Abdin, Z., et al., *Hydrogen as an energy vector.* Renewable and sustainable energy reviews, 2020. **120**: p. 109620.
19. Jiang, L., et al., *Surface wettability engineering: CoSx-Ni3S2 nanoarray electrode for improving overall water splitting.* Applied Catalysis B: Environmental, 2020. **269**: p. 118780.
20. Ghazvini, M., et al., *Geothermal energy use in hydrogen production: A review.* International Journal of Energy Research, 2019. **43**(14): p. 7823-7851.
21. Ng, B.J., et al., *Z-scheme photocatalytic systems for solar water splitting.* Advanced Science, 2020. **7**(7): p. 1903171.
22. McHugh, P.J., A.D. Stergiou, and M.D. Symes, *Decoupled electrochemical water splitting: from fundamentals to applications.* Advanced Energy Materials, 2020. **10**(44): p. 2002453.
23. Zhang, L., et al., *Recent advances in 1D electrospun nanocatalysts for electrochemical water splitting.* Small Structures, 2021. **2**(2): p. 2000048.
24. Li, L., et al., *Metallic nanostructures with low dimensionality for electrochemical water splitting.* Chemical Society Reviews, 2020. **49**(10): p. 3072-3106.
25. Hu, X., et al., *Nickel foam and stainless steel mesh as electrocatalysts for hydrogen evolution reaction, oxygen evolution reaction and overall water splitting in alkaline media.* RSC advances, 2019. **9**(54): p. 31563-31571.
26. Sultan, S., et al., *Single atoms and clusters based nanomaterials for hydrogen evolution, oxygen evolution reactions, and full water splitting.* Advanced Energy Materials, 2019. **9**(22): p. 1900624.
27. Yang, L., et al., *Active site identification and evaluation criteria of in situ grown CoTe and NiTe nanoarrays for hydrogen evolution and oxygen evolution reactions.* Small Methods, 2019. **3**(5): p. 1900113.
28. Jaschin, P.W., et al., *A materials perspective on magnesium-ion-based solid-state electrolytes.* Journal of Materials Chemistry A, 2020. **8**(6): p. 2875-2897.
29. Kim, S., N.T. Nguyen, and C.W. Bark, *Ferroelectric materials: a novel pathway for efficient solar water splitting.* Applied Sciences, 2018. **8**(9): p. 1526.
30. Yu, J., et al., *Recent advances and prospective in ruthenium-based materials for electrochemical water splitting.* Acs Catalysis, 2019. **9**(11): p. 9973-10011.
31. Liu, Y., et al., *Research progress of oxygen evolution reaction catalysts for electrochemical water splitting.* ChemSusChem, 2021. **14**(24): p. 5359-5383.
32. Cui, B. and G.-D. Fu, *Process of metal− organic framework (MOF)/covalent− organic framework (COF) hybrids-based derivatives and their applications on energy transfer and storage.* Nanoscale, 2022.
33. Sun, Y., et al., *Compositional engineering of sulfides, phosphides, carbides, nitrides, oxides, and hydroxides for water splitting.* Journal of Materials Chemistry A, 2020. **8**(27): p. 13415-13436.

34. Sun, H., et al., *Self-supported transition-metal-based electrocatalysts for hydrogen and oxygen evolution.* Advanced Materials, 2020. **32**(3): p. 1806326.
35. Zhou, D., et al., *Recent advances in non-precious metal-based electrodes for alkaline water electrolysis.* ChemNanoMat, 2020. **6**(3): p. 336-355.
36. Marini, S., et al., *Advanced alkaline water electrolysis.* Electrochimica Acta, 2012. **82**: p. 384-391.
37. Wang, J., et al., *Carbon-based electrocatalysts for sustainable energy applications.* Progress in Materials Science, 2021. **116**: p. 100717.
38. Wang, Y., et al., *Reduced mesoporous Co3O4 nanowires as efficient water oxidation electrocatalysts and supercapacitor electrodes.* Advanced Energy Materials, 2014. **4**(16): p. 1400696.
39. Ma, T.Y., S. Dai, and S.Z. Qiao, *Self-supported electrocatalysts for advanced energy conversion processes.* Materials Today, 2016. **19**(5): p. 265-273.
40. Chen, H., et al., *Active site engineering in porous electrocatalysts.* Advanced Materials, 2020. **32**(44): p. 2002435.
41. Kong, L., et al., *Electrochemically active sites inside crystalline porous materials for energy storage and conversion.* Chemical Society Reviews, 2020. **49**(8): p. 2378-2407.
42. Jin, Y., et al., *Porous MoO2 nanosheets as non-noble bifunctional electrocatalysts for overall water splitting.* Advanced Materials, 2016. **28**(19): p. 3785-3790.
43. Ipadeola, A.K., et al., *Porous High-Entropy Alloys as Efficient Electrocatalysts for Water-Splitting Reactions.* Electrochemistry Communications, 2022: p. 107207.
44. Shrivastava, S., N. Jadon, and R. Jain, *Next-generation polymer nanocomposite-based electrochemical sensors and biosensors: A review.* TrAC Trends in Analytical Chemistry, 2016. **82**: p. 55-67.
45. Msheik, M., S. Rodat, and S. Abanades, *Methane cracking for hydrogen production: a review of catalytic and molten media pyrolysis.* Energies, 2021. **14**(11): p. 3107.
46. Zheng, G., et al., *Tungsten oxide nanostructures and nanocomposites for photoelectrochemical water splitting.* Nanoscale, 2019. **11**(41): p. 18968-18994.
47. Nisar, L., et al., *Ultrathin CoTe nanoflakes electrode demonstrating low overpotential for overall water splitting.* Fuel, 2020. **280**: p. 118666.
48. Wang, X., et al., *Metal–organic framework derived CoTe 2 encapsulated in nitrogen-doped carbon nanotube frameworks: a high-efficiency bifunctional electrocatalyst for overall water splitting.* Journal of Materials Chemistry A, 2018. **6**(8): p. 3684-3691.
49. Liu, X., et al., *Bi2Zr2O7 nanoparticles synthesized by soft-templated sol-gel methods for visible-light-driven catalytic degradation of tetracycline.* Chemosphere, 2018. **210**: p. 424-432.
50. Wang, R., et al., *Copper Telluride Nanosheet/Cu Foil Electrode: Facile Ionic Liquid-Assisted Synthesis and Efficient Oxygen Evolution Performance.* The Journal of Physical Chemistry C, 2020. **124**(40): p. 22117-22126.

51. Bhat, K.S., H.C. Barshilia, and H. Nagaraja, *Porous nickel telluride nanostructures as bifunctional electrocatalyst towards hydrogen and oxygen evolution reaction.* international journal of hydrogen energy, 2017. **42**(39): p. 24645-24655.
52. Qin, Q., et al., *Ionic liquid-assisted synthesis of Cu7Te4 ultrathin nanosheets with enhanced electrocatalytic activity for water oxidation.* Nano Energy, 2017. **41**: p. 780-787.

Figures

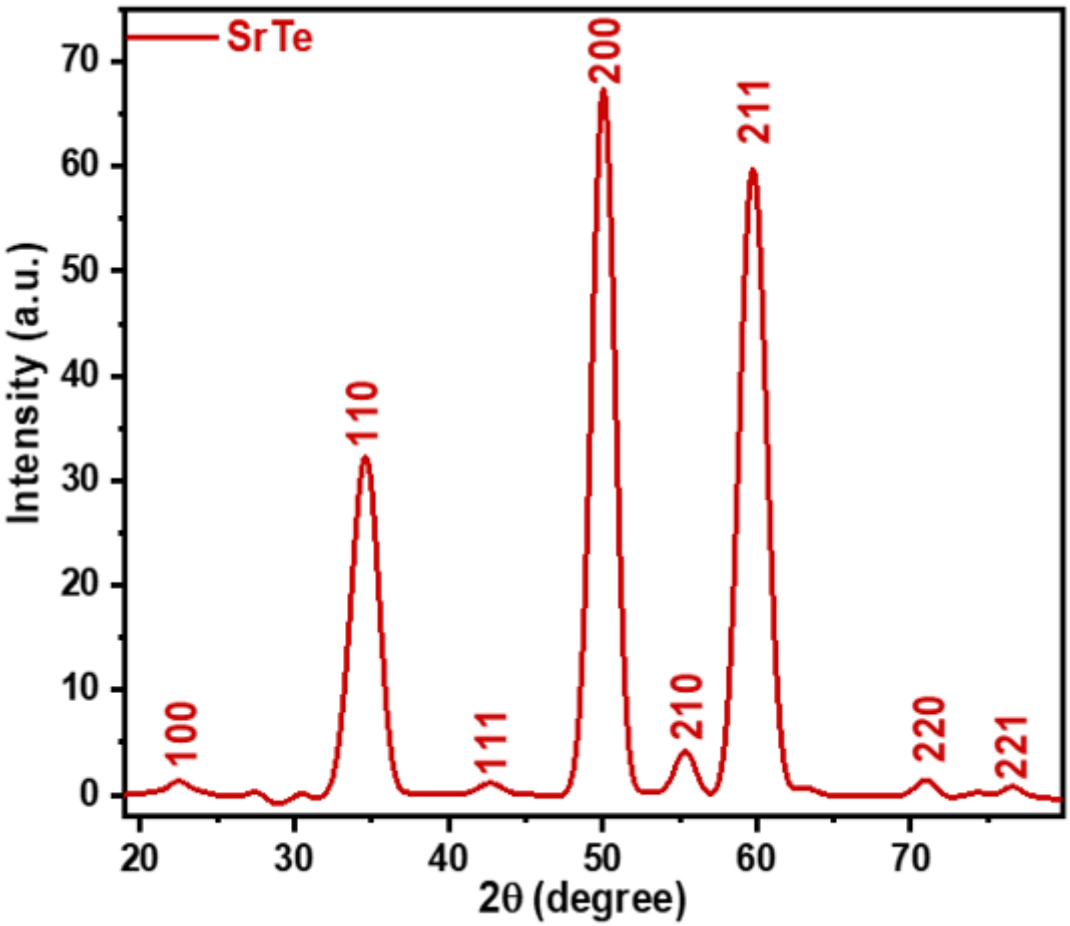

Figure 1

XRD spectra of synthesized SrTe/GC

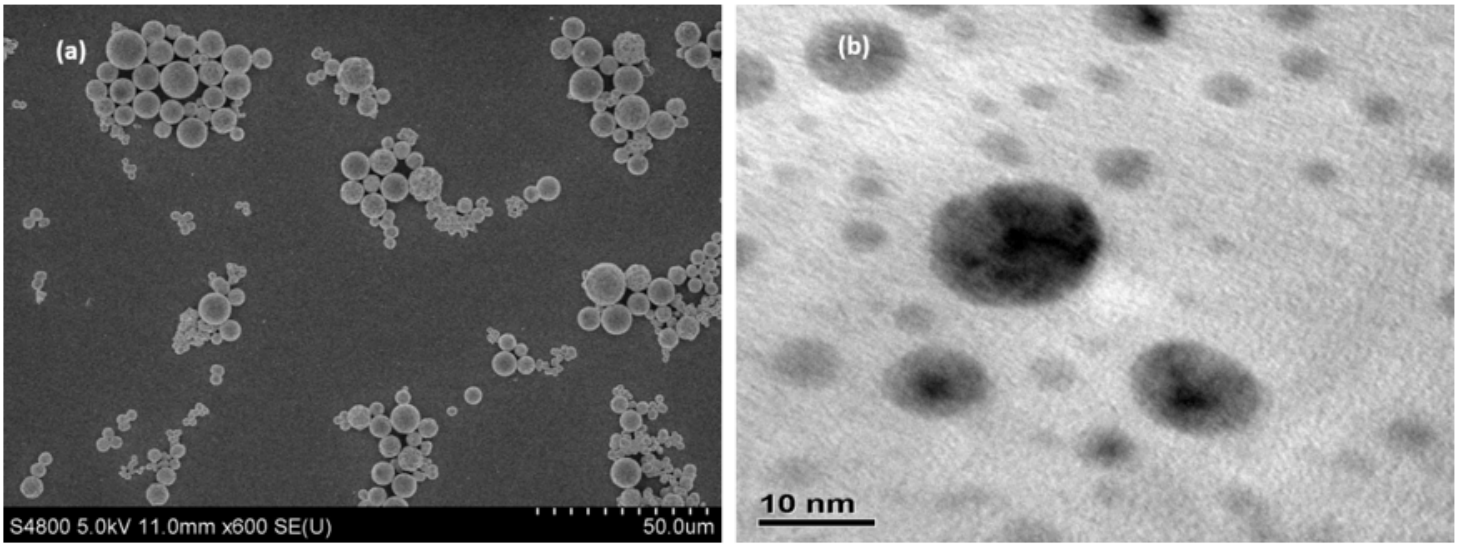

Figure 2

(a) SEM, and (b) TEM micrographs of SrTe/GC

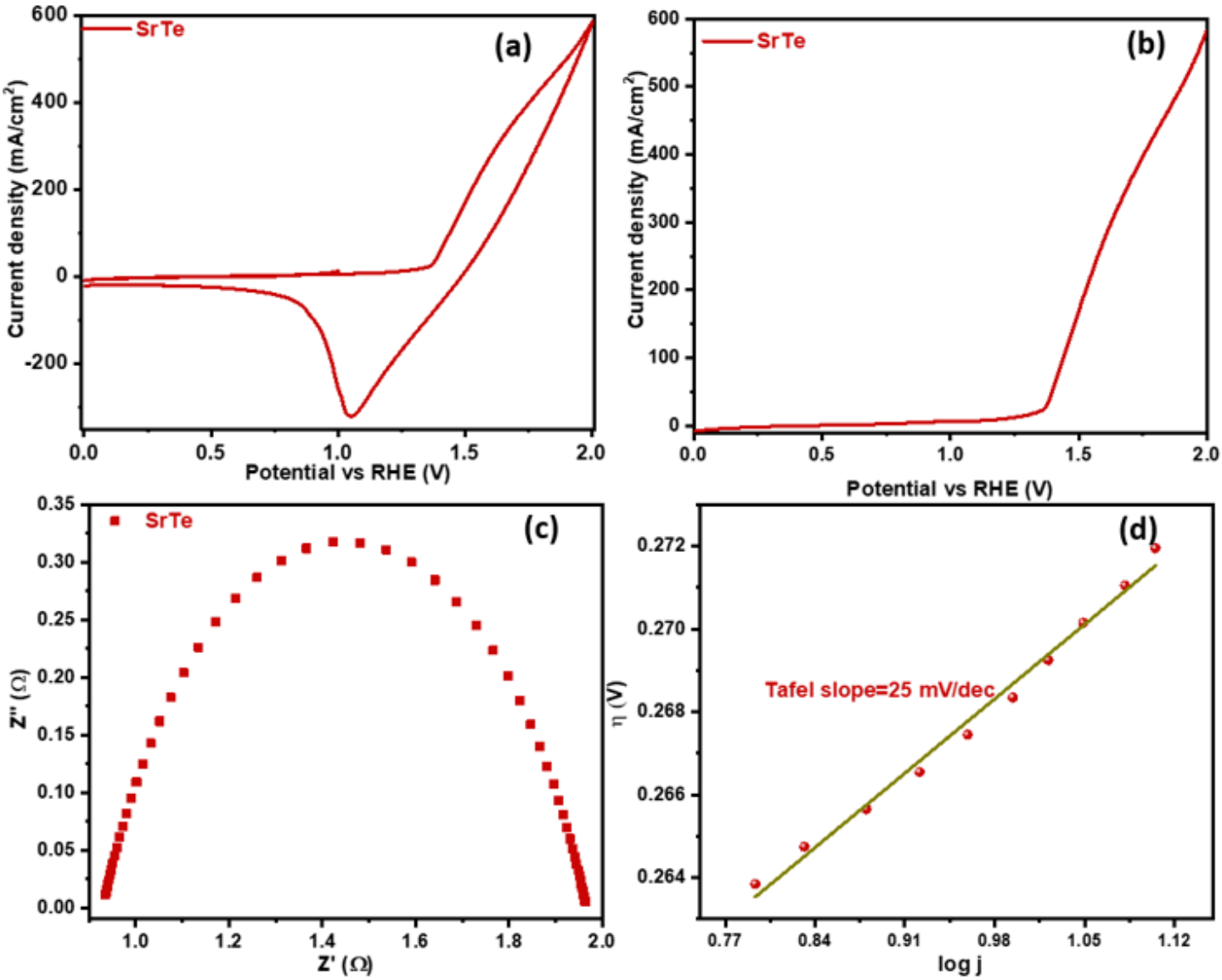

Figure 3

(a) cyclic voltammogram, (b) linear sweep voltammogram, (c) EIS, (d) tafel slope of SrTe

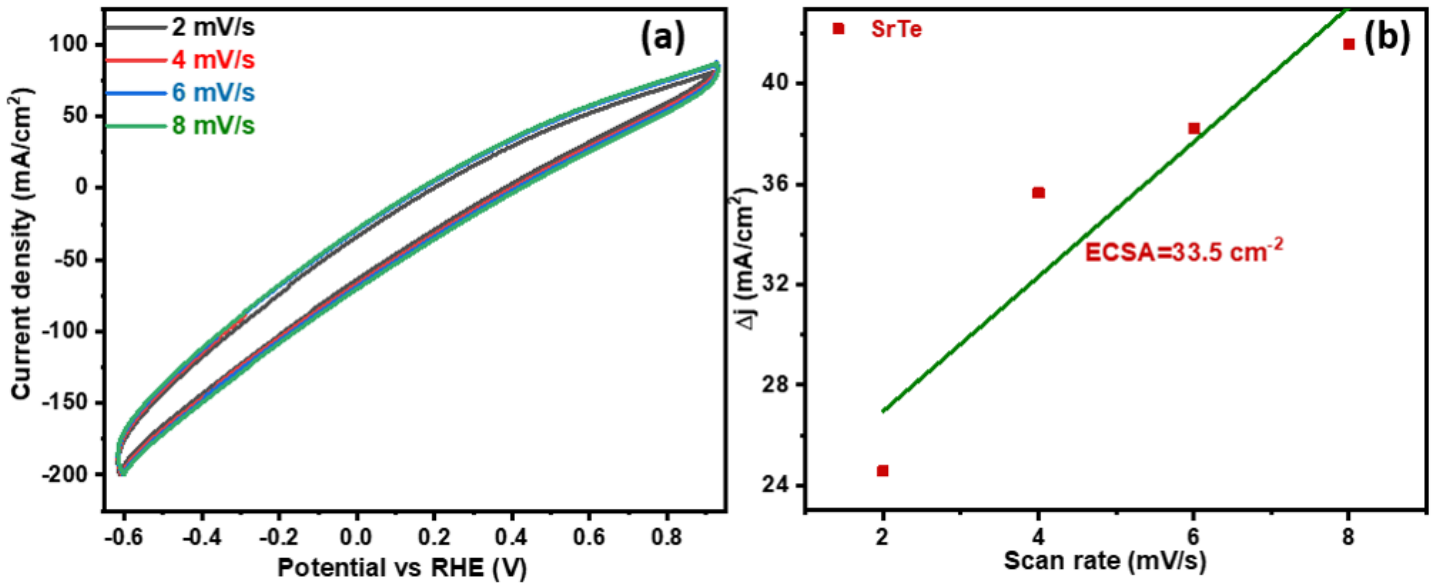

Figure 4

(a) ECSA plot, (b) C_{dl} values of SrTe

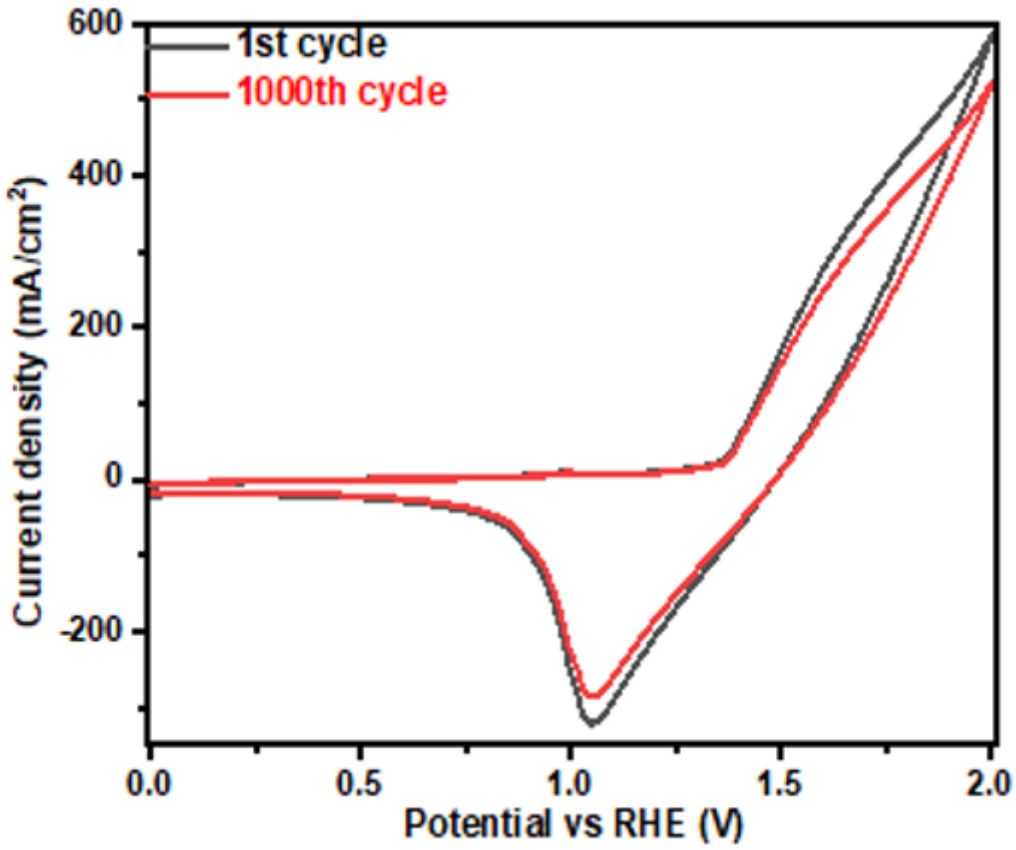

Figure 5

Cyclic stability of SrTe/GC

Supplementary Files

This is a list of supplementary files associated with this preprint. Click to download.

- GA.png
- scheme1.png